Acoustic Near-Field Properties Associated with Broadband Shock Noise

John M. Seiner* and James C. Yu*
NASA Langley Research Center, Langley, Virginia

Shock noise associated with unheated supersonic jets was investigated using a near-field microphone array and a single-sensor wedge-shaped hot-film probe. Both over- and underexpanded cases were investigated using Mach 1.45 and 1.99 convergent-divergent nozzles. Correlation measurements through each shock cell of a single underexpanded case with the Mach 1.45 nozzle were obtained between the hot-film probe and the microphone array. The results of the hot-film/near-field microphone correlations show general agreement with certain theoretical models as to the location for shock noise production, and provide evidence for the existence of some large-scale flow structure that collectively interacts and phases the motion of the downstream shocks. The near-field microphone correlations demonstrate that downstream shocks dominate shock noise production and suggest the existence of a Doppler effect in the near field of the sources. In addition, broadband shock noise is found to propagate at small angles to the jet axis.

Introduction

THE present study was initiated as an extension to the research results obtained in an earlier investigation by Seiner and Norum.[1] The results of the previous study indicated that 1) the broadband shock noise amplitude correlated well with the strength of downstream shocks, 2) this noise originated in the vicinity of the oblique compression shocks, 3) the significant turbulence length scale exceeded one shock cell length, and 4) the shock noise source intensity for a given shock interface was proportional to the local thickness of the supersonic portion of the mixing layer.

Except for the shock noise amplitude behavior, these experimental results were obtained through the use of a single correlating near-field microphone and a wedge-shaped hot-film probe. The near-field microphone was positioned axially and above the first and then third shock termination of an underexpanded flowfield produced by a Mach 2 covergent-divergent nozzle. The hot-film probe was located at various axial and radial locations through the compression and expansion zones of the first and third shock cells.

The objectives of this experimental study are to examine in more detail the principal findings of the previous study and, in particular, to determine more clearly if a preferred region exists for the production of broadband shock noise. To the extent possible, the local aerodynamic properties associated with such a preferred region are also of interest in the sense that the various analytical broadband shock noise models proposed[2-7] differ as to their interpretation of the aerodynamic source for shock noise production. Thus, the objectives of this experimental study would provide an improved perspective for examining these various analytical models.

In the present study, a near-field array of microphones was positioned along the jet axis at a fixed radial location. The near field is taken as that region within an acoustic wavelength of any source. With the array, it was possible to obtain improved resolution over the previous study for determining multiple shock noise source locations. Mutual correlations between the microphones in the near-field array also provided a means for identifying propagating paths for the broadband shock noise component as well as those due to screech and jet noise. In certain cases, where the broadband shock noise component dominated a spectral band, the near-field array was also correlated with a far-field microphone to estimate the region for maximum shock noise emission. The hot-film probe was simultaneously correlated with all microphone elements in the array to estimate the location of the aerodynamic source region for shock noise generation. In contrast to the previous study,[1] the near-field array also permitted determination of the wedge hot-film probe's sound field, which appears as a contaminating component to the measurements.

The research results of this study were primarily obtained using the underexpanded flowfield generated by a Mach 1.45 convergent-divergent nozzle operating at a nozzle exit to ambient static pressure ratio of $P_e/P_a = 1.69$. Several other nozzle pressure ratios, including overexpanded cases, were examined with this nozzle as well as a Mach 1.99 convergent-divergent nozzle using only the near-field array of microphones. The results demonstrate the influence of the shock-wave field on the axial development of turbulence, reconfirm the findings of Ref. 1 that shock noise is produced near oblique compression shocks, and show that the majority of broadband shock noise in both over- and underexpanded flows occurs in the vicinity of shocks near the end of the initial mixing layer. Additionally, it is found that in this region shocks appear to interact collectively with some large-scale turbulent motion in the shear layer. Near-field microphone correlations and spectra indicate the presence of the Doppler factor in the near field of the shock sources. These results indicate that the Doppler factor originates from a convecting acoustic disturbance rather than from a phased array of acoustic sources as modeled, for example, by Harper-Bourne and Fisher.[4] The near-field microphone correlations also show that the broadband shock noise source radiates a component at small angles to the jet axis.

Description of Experimental Configuration

The experiment was conducted in one of NASA Langley's large anechoic facilities. Both the Mach 1.45 and 1.99 convergent-divergent nozzles' near-field acoustic behavior was examined over an extensive pressure ratio range with and without the presence of a probe in the flowfield. In terms of the ratio of the nozzle exit pressure to the ambient static

Presented as Paper 81-1975 at the AIAA Seventh Aeroacoustics Conference, Palo Alto, Calif., Oct. 5-7, 1981; submitted Oct. 22, 1981; revision received Nov. 18, 1983.

*Research Scientist, Acoustic and Noise Reduction Division. Member AIAA.

pressure, the pressure range varied at $0.13 \le P_e/P_a \le 5.36$. The respective exit diameters for these nozzles were 4.268 and 4.989 cm. As shown in Fig. 1, 11 near-field microphones were positioned at $R/D = 2.68$ parallel to the jet axis. The axial and radial positions of these microphones remained fixed throughout the experiment. These positions were selected so that at least one microphone would be located approximately normal to the first six shock terminations when the Mach 1.45 nozzle was operated underexpanded at $P_e/P_a = 1.69$. The locations for these shock terminations are illustrated in Fig. 1 as those positions along the sonic line where a shock reflection occurs. In a similar fashion, a near-field array of nine microphones was used for the Mach 1.99 flow, enabling the study of its first four shock terminations when it was operated underexpanded at $P_e/P_a = 1.47$. The relevant locations for shock terminations and microphone positions are listed in Table 1 for each nozzle.

Flow measurements were acquired using supersonic static and total pressure probes and a commercial wedge-shaped hot-film probe with a 40-deg half-angle. These same probes were used in the previous study reported in Ref. 1. The measurements with the hot-film probe in this study were confined to the flow condition obtained with the Mach 1.45 nozzle operating underexpanded at $P_e/P_a = 1.69$. Both the longitudinal turbulent velocity and fluctuating temperature components were measured at 93 radial and axial locations in the flow at 3 film overheat ratios and simultaneously correlated with each of the 11 near-field microphones. Only the 39 axial probe locations $1 \le x/D \le 12$ at $R/D = 0.45$ are reported in this study.

In addition to the near-field microphone array, the experiment also included a far-field microphone positioned at 90 deg to the jet axis at $R/D = 61.5$ for the Mach 1.45 nozzle and $R/D = 52.6$ for the Mach 1.99 nozzle. This microphone was simultaneously correlated with all the near-field microphones and the hot-film probe when using the Mach 1.45 nozzle. Prior to the initialization of these experiments, a far-field array of microphones was utilized to obtain far-field spectra to establish the convection Mach number through the observed Doppler factor for broadband shock noise. The far-field microphone array was arc centered on the nozzle exit with a radius of 3.05 m.

Interpretation of Wedge Hot-Film Response

The convective heat-transfer behavior of the 40-deg half-angle wedge hot-film probe differs significantly in supersonic flow (see Seiner[8]) from that which is observed for cylindrical-type sensors. The convective heat-transfer coefficient for cylindrical sensors (see Morkovin[9]) depends on a Reynolds number based on stagnation temperature conditions. Its dependence on Mach number is small and customarily neglected for freestream Mach numbers exceeding 1.3 (see Rose[10]). Instead, the wedge-type sensor's convective heat-transfer coefficient exhibits a response with Reynolds number based on freestream static temperature. This difference in response leads to a substantial modification of the wedge probe's functional dependence on the flow parameters. For example, Ref. 8 shows that the wedge probe has a greater sensitivity to velocity than to either density or pressure for freestream Mach numbers to at least $M = 2.5$ for all probe temperature overheats. Additionally, it is shown that the wedge probe's sensitivity to either density or pressure exhibits a very weak dependence on probe temperature overheat and that the probe's temperature recovery ratio η is essentially independent of freestream Reynolds number Re_∞. These observations lead to the following method for interpreting the measured mean square voltage fluctuations $\overline{e'^2}$ for a wedge-type probe[8]:

$$\frac{\overline{e_c'^2}}{E_b^2} = S_u^2 \frac{\overline{u'^2}}{U^2} - 2S_u S_T \frac{\overline{u'T_0'}}{UT_0} + S_T^2 \frac{\overline{T_0'^2}}{T_0^2} \tag{1}$$

where the sensitivities to pressure S_p, velocity S_u, and temperature S_T are given by

$$S_p = \frac{1}{2} \frac{\partial(\ln Nu_0)}{\partial(\ln Re_\infty)} \tag{2}$$

$$S_u = \alpha_1 S_p - \frac{1}{2\alpha_0 \tau_{wr}} \frac{\partial(\ln \eta)}{\partial(\ln M)} \tag{3}$$

$$S_T = \left(1 + \frac{m_0}{\alpha_0} - \frac{\alpha_1}{2}\right) S_p + \frac{1}{2}\left(S_u + \frac{1}{\tau_{wr}} + \frac{\partial(\ln Nu_0)}{\partial(\ln \theta)} - n_0\right) \tag{4}$$

In Eq. (1) the corrected mean square voltage $\overline{e_c'^2}$ is determined from measured voltage fluctuations e' by a concomitant measure of the wedge probe's fluctuating voltage contribution e_p' due to pressure. The corrected mean square voltage can be expressed as

$$\overline{e_c'^2} = \overline{(e' - e_p')^2} \tag{5}$$

where the fluctuating voltage contribution due to pressure is given by

$$e_p' = E_b S_p p'/P \tag{6}$$

In the above equations, the time-dependent pressure, velocity, and temperature are represented by p', u', and T_0' with

Table 1 Shock termination and near-field microphone locations

Shock termination	x/D	Microphone No.	x/D
[a]Mach 1.45 nozzle (tab inserted at $P_e/P_a = 1.69$)			
1	1.99	1	0.00
2	3.70	2	2.00
3	5.50	3	3.04
4	7.00	4	4.07
5	9.00	5	5.08
6	10.50	6	6.09
7	11.75	7	7.05
		8	8.00
		9	8.93
		10	9.87
		11	11.56
Mach 1.99 nozzle (no tab at $P_e/P_a = 1.47$)			
1	2.55	1	0.00
2	5.60	2	1.30
3	8.20	3	2.60
4	10.72	4	4.10
5	13.12	5	5.60
6	15.37	6	6.92
7	17.50	7	8.25
8	19.45	8	9.51
		9	10.76

[a]In this case there are three more shock terminations that can be observed before reaching the end of the supersonic core.

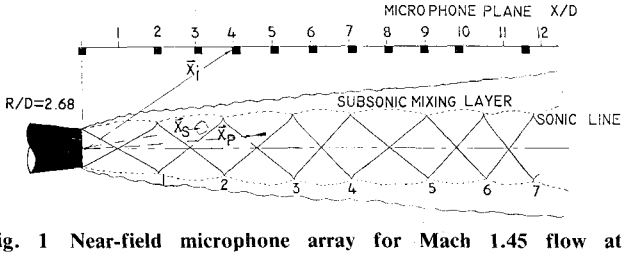

Fig. 1 Near-field microphone array for Mach 1.45 flow at $P_e/P_a = 1.69$.

corresponding mean values given by P, U, and T_0. The Nusselt number is represented by Nu_0, the mean anemometer voltage by E_b, the temperature overheat by θ, and the temperature loading by τ_{wr}. Both m_0 and n_0 are taken to be constants with numerical values of 0.765 and 0.885, respectively. The parameters α_0 and α_1 are functions of Mach number and are given by the auxiliary equations.

$$\alpha_0 = \left(1 + \frac{\gamma - 1}{2} M^2\right)^{-1} \tag{7}$$

$$\alpha_1 = 1 + m_0(\gamma - 1)M^2 \tag{8}$$

For the purposes of this study, mildly over- and underexpanded flows are considered to be sufficiently isoenergetic and the freestream Mach numbers to be sufficiently high to assume that the e_p' voltage contribution is negligible. These conditions are essentially satisfied by selecting the underexpanded nozzle exit static pressure ratio of $P_e/P_a = 1.69$ for the wedge hot-film probe measurements of the Mach 1.45 nozzle plume.

Results

General Acoustic Features

This section discusses several of the experimental problems encountered with the near-field study of supersonic jets when multiple sound source components are active. These problems are essentially associated with attempting to find a flowfield condition that maximizes the contribution of the source component of interest, which in this study is broadband shock noise. At the same time, the selected flowfield condition should not substantially compromise the quality of the hot-film flow measurements.

In the previous study[1] as well as this one, underexpanded flowfield conditions are selected to avoid aerodynamic measurements with mixed flows (i.e., subsonic-supersonic domains) that occur when operating a supersonic nozzle overexpanded. Far-field acoustic measurements of overall sound pressure level are used to establish the underexpanded condition for each supersonic nozzle that maximizes the contribution of shock noise relative to jet mixing noise.

Figure 2 shows an estimate for the amplitude of the broadband shock noise radiated to the acoustic far field ($R/D = 80$) at 90 deg to the jet axis for several supersonic nozzles. These data are derived from measured overall sound pressure levels and an estimate of the jet noise contribution using the recommended procedure of Stone.[11] The screech mode is suppressed when it would contribute to the overall measured level. The data are presented as a function of each nozzle's ratio of exit static to ambient pressure to normalize the results obtained for the various supersonic nozzles. Overexpanded conditions occur when $P_e/P_a < 1$ and underexpanded conditions occur when $P_e/P_a > 1$. At each nozzle's design point (i.e., $P_e/P_a = 1$) the estimated broadband shock noise amplitude is negligible, demonstrating a good agreement between Stone's predicted jet noise levels and those measured in these experiments. The amplitude variation of broadband shock noise indicates that considerably more shock noise is produced in the underexpanded mode and that for this mode maximum shock noise levels occur between $P_e/P_a = 1.5$ and 2.0 for all three supersonic nozzles. On the basis of this information, the respective conditions of $P_e/P_a = 1.69$ and 1.47 are selected for the $M_e = 1.45$ and 1.99 supersonic nozzles as the candidate conditions for the simultaneous measurements of flow and acoustic data. This selection permits a simplification to the interpretation of the wedge hot-film response that occurs with high freestream Mach numbers.

However, a serious disadvantage exists in restricting the measurements to underexpanded conditions. In the underexpanded conditions, both the jet noise and screech components have spectral scales that more closely approach those observed for the broadband shock noise component. This occurs because, with increasing nozzle pressure ratios, the peak frequency for jet noise increases while the broadband peak shock noise frequency decreases due to the expanding shock cell length. Even though the screech component decreases with increasing nozzle pressure ratio, its variation is less than the broadband component. This means that for the

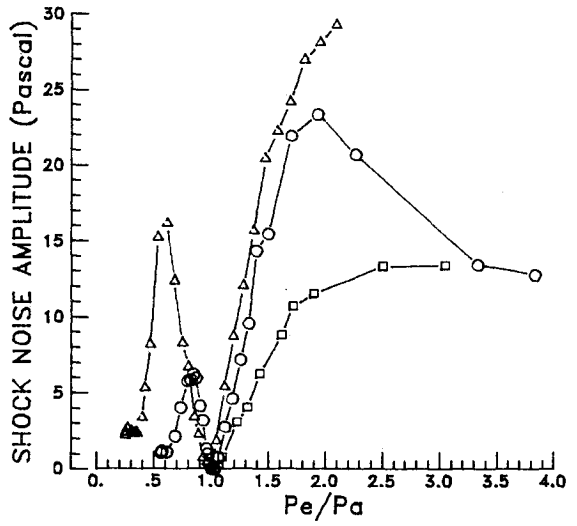

Fig. 2 Estimated broadband shock noise (□ $M_e = 1.0$, ○ $M_e = 1.45$, △ $M_e = 1.99$).

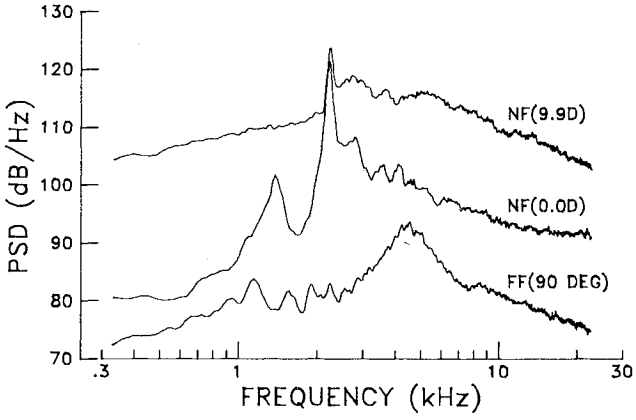

a) $P_e/P_a = 1.69$ (underexpanded).

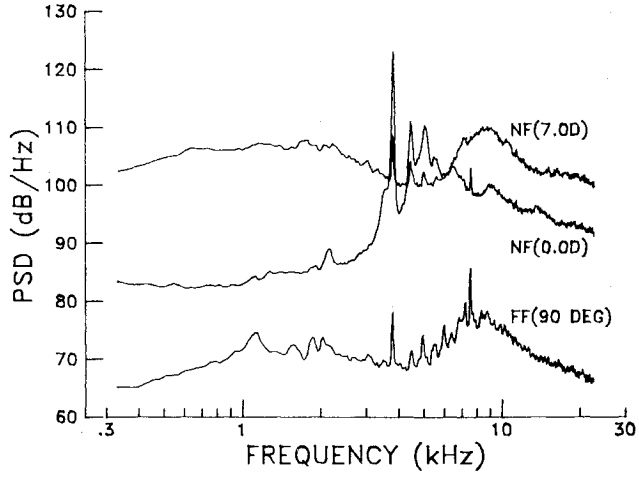

b) $P_e/P_a = 0.79$ (overexpanded).

Fig. 3 Near- and far-field acoustic spectra for $M_e = 1.45$ nozzle without screech suppression.

candidate underexpanded conditions selected, the jet noise component will dominate the downstream microphones, whereas the screech component will highly influence the upstream near-field microphones. This general feature can be observed in the example narrowband spectra shown in Fig. 3.

In Fig. 3a the characteristic broadband shock noise spectrum is shown in comparison with two near-field spectra for the candidate underexpanded case of $P_e/P_a = 1.69$ for the Mach 1.45 nozzle. The far-field spectrum is for the observation angle of 90 deg to the jet axis. In this case, the screech component is not suppressed and, while no clear screech tone can be observed in the far-field data, screech is readily apparent in the near-field spectra. Comparing the two near-field spectra at microphone positions 1 and 9 (see Table 1 for microphone positions), it is clear that the amplitude of the screech component is nearly equivalent, but a large increase in the jet noise almost masks off this component at the downstream microphone location. In this case, near-field correlations between upstream and downstream microphone pairs reveal sound waves propagating upstream identifiable as the screech component and waves traveling downstream identifiable as the jet noise component.

The narrowband spectra of Fig. 3b at the overexpanded condition of $P_e/P_a = 0.79$ for this same nozzle show that the jet noise component peaks at a much lower frequency and that the broadband shock noise peaks at a higher frequency than was observed in the underexpanded condition. This result is achieved by a lower fully expanded velocity, reducing the jet noise peak frequency and amplitude, and a corresponding decrease in the shock cell spacing, resulting in an increase in the peak frequency of the near-field broadband shock noise. This is demonstrated by the near-field spectrum at microphone position 7. In this case, near-field correlations are dominated by the broadband shock noise process, particularly when the screech component is suppressed. In this instance, it is also possible to obtain good correlation between near- and far-field microphones.

From the near-field data of Fig. 3, it was evident that suppression of the screech mode was desirable so that better definition of the broadband shock noise component could be obtained. For this purpose a tab, previously used and described in Ref. 12, was inserted at the nozzle exit. While this research reported reductions of the screech mode below other spectral components as shown in the far-field spectra of Fig. 4, complete reduction of this mode did not occur as shown by the near-field comparisons in this figure. With this tab inserted at the nozzle exit, the upstream near-field microphones were still influenced by screech, but the downstream microphones were dominated by the broadband shock noise component in overexpanded conditions and by jet noise in underexpanded conditions. Therefore, studying broadband shock noise in the underexpanded condition required at least a correlation between the supersonic flow features and the near-field microphones.

Supersonic Mean and Turbulent Flow Properties

When the screech mode is suppressed, as with the use of a tab, the shock wavelength is reduced as has been previously reported by Norum and Seiner.[12] Their data show that, except for the first shock cell, there is an approximately 10% reduction in the shock wavelength when screech is suppressed by a tab device. Since only 39 axial stations were examined during the course of this investigation, the locations for compression and expansion regions through the first 7 shock cells are known with limited precision. In addition, there is an accompanying alteration in the relative observation angles between the near-field microphones and plume shock-wave structure.

In order to solve for the fluctuating flow variables, the hot-film sensitivity equations require an independent measure of the freestream Mach number. The freestream Mach number variation for the 39 axial locations in the supersonic shear layer at $R/D = 0.45$ is shown in Fig. 5. In this figure the start of a compression region occurs at those points where the Mach number begins to decrease and the start of an expansion zone at those points where the Mach number begins to increase. The locations where shocks terminate in the shear layer occur at R/D values slightly greater than 0.45, but would closely correspond to the minimum peaks shown in Fig. 5. These values are tabulated in Table 1 along with the axial locations of the near-field microphones.

Figure 5 shows that the axial range of the data covers the first seven shock cells and that the minimum Mach number throughout the entire range is 1.5. On the basis of these data and the wedge probe's sensitivity equations (2-4), the fluctuating voltage contribution e_p' due to pressure is expected to be relatively small. In this investigation, 3 temperature overheats ($\tau = 0.2, 0.35, 0.5$) were used to solve Eq. (1) for the longitudinal velocity and total temperature fluctuations for the 39 axial stations in Fig. 5. The result of these calculations is shown in Fig. 6.

The turbulent velocity fluctuations have been normalized by the jet exit velocity and the total temperature fluctuations by the stagnation temperature, which in the current tests was within 2°C of the surrounding ambient medium. It is evident from these data that the velocity fluctuations are typically an order of magnitude larger than the total temperature fluctuations. One expects then that correlations between the hot-film probe and near-field microphones may be dominated by

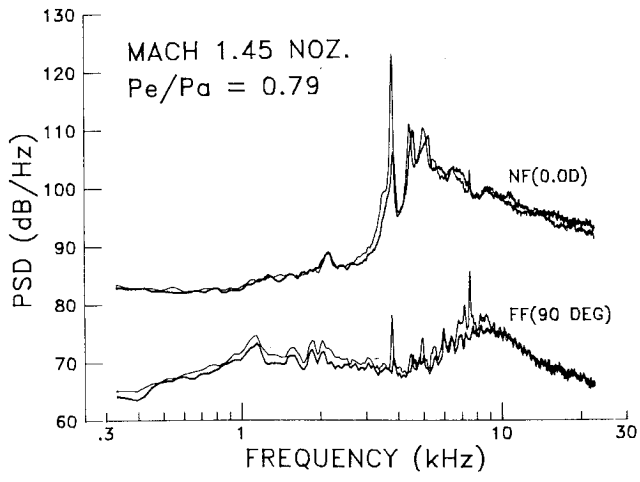

Fig. 4 Near- and far-field acoustic spectra with screech (— unsuppressed, — suppressed).

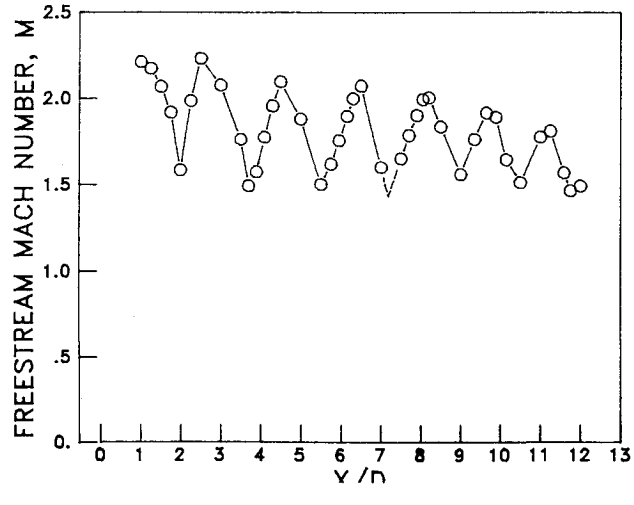

Fig. 5 Mach number variation for $M_e = 1.45$ jet flow at $P_e/P_a = 1.69$ and $R/D = 0.45$.

the coherence between the velocity and acoustic pressure fluctuations.

The turbulent velocity fluctuations of Fig. 6 show that there is a strong modulation to the growth of the mixing layer as convecting flow disturbances are transported through the compression and expansion zones of each shock cell. The peak velocity fluctuations occur at the end of each compression zone and the minima occur at the end of each expansion zone. The nature of the process appears to be governed by variations of the mean flowfield through each shock cell. This feature can be understood on the basis that the mean streaming motion in a compression zone converges the same mass flux into a smaller unit volume. Random disturbances distributed over a much larger unit volume upstream of the compression shock are then transported into this smaller unit volume. Due to conservation of angular momentum, the detected turbulence level is increased. This viewpoint suggests that alterations to disturbances that convect through and interact with a weak shock are of lesser significance than those produced by variations in the mean flowfield.

Shock Noise Source Location

On the basis of the theory for vortex shock interaction[3,13] and the prior research in Ref. 1, we expect that shock noise is produced in the vicinity of oblique compression shocks. This concept is re-examined using simultaneous correlations between the hot-film wedge probe and near-field microphone array. The 39 axial stations, for which turbulent velocity fluctuations were acquired, form the base for this study. As mentioned previously, this method is adopted for source location since jet noise dominates the near-field microphone correlations in the underexpanded mode.

In performing these correlations, however, there is another identifiable mechanism present that alters the nature of the correlation method. This mechanism appears to be related to noise associated with the film probe being inserted into a supersonic region of the flow. At certain angles downstream of the hot-film probe's position, the correlation function obtained with microphones in that region appear to have a shape like that expected for a dipole-type noise source. In these instances, the observed time delays for the correlation predict precisely the room temperature sonic speed. This noise source is more easily identifiable in the tests conducted with the Mach 1.45 nozzle as compared to that associated with the Mach 1.99 nozzle. Figure 7 shows the basic pattern exhibited by this additional noise component. The amplitude levels for the beam pattern are relative and are estimated from the local slope of the skewed correlation function at the zero crossing level. Evidently the beam pattern for this mechanism is rather narrow and confined to a region within the Mach angle for the probe. The Mach 2 case shows a similar feature, but is generally weaker and has its beam pattern rotated further downstream. On the basis of this additional problem, correlations with microphones downstream of the probe's position in the flow were eliminated from consideration.

The location for broadband shock noise is estimated on the following basis. Correlations of a near-field microphone with the hot-film probe at several downstream axial stations produce a set of solutions that satisfy the optimized time delay equation,

$$\tau_i = |X_s - X_i|/c_0 + (X_s - X_p)\cdot e_x/U_c \qquad (9)$$

where c_0 and U_c are, respectively, the ambient sound speed and disturbance convection velocity. Figure 1 denotes the general geometry. Equation (9) assumes that, once generated, the sound waves propagate directly to the near-field receivers at sonic speed and that flow disturbances are convected to the film probe at a constant speed. In order to simplify the procedures, it is further assumed that the significant event occurs in the azimuthal plane between the microphone array and film probe. Using the geometrical arrangement of Fig. 1 and dropping any azimuthal dependence, Eq. (9) can be expressed as

$$(1-M_c^2)\xi^2 - M_c^2\eta^2 + 2M_c(M_c a_i - d_i)\xi + 2b_i M_c^2\eta + M_c^2(d_i^2 - a_i^2 - b_i^2) = 0 \qquad (10)$$

where $\xi=(X_s-X_p)/D$, $\eta=(r_s-r_p)/D$, and a_i and b_i are coefficients expressing the axial and radial distance, respectively, between the probe and near-field microphone. In Eq. (10), the nondimensional optimized time delay $d_i=c_0\tau/D$ and the convection Mach number $M_c=U_c/c_0$. For every given optimal time delay, a curve is generated by Eq. (10) along which a possible position for the shock noise source exists. The region where these curves intersect or focus identifies the region for broadband shock noise production.

The nature of the curves generated by Eq. (10) are highly dependent on the choice for the convection Mach number. Therefore, it is necessary to derive an initial estimate for the convection Mach number that has a physical bearing on the problem. This can be done by using the observed far-field behavior of the peak broadband shock noise frequency as a function of observation angle θ to the jet axis. According to Harper-Bourne and Fisher,[4] the peak frequency for broadband shock noise at non-normal viewing angles is related to the peak frequency at 90 deg through the Doppler

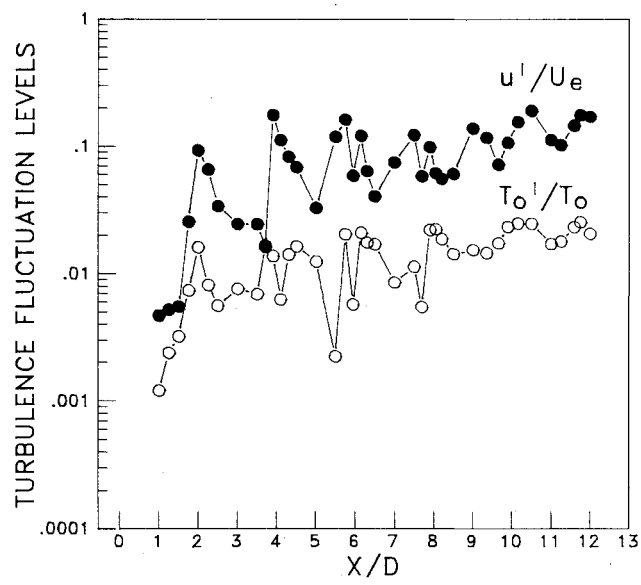

Fig. 6 Axial evolution of turbulence fluctuation levels for $M_e = 1.45$ flow at $P_e/P_a = 1.69$ (• u'/U_e, ○ T_0'/T_0).

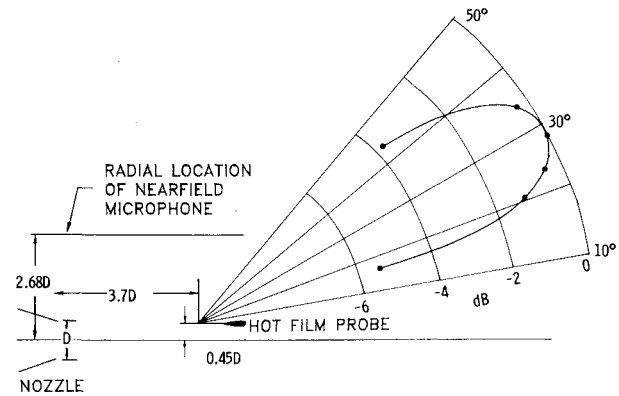

Fig. 7 Directional distribution of probe noise component for $M_e = 1.45$ jet at $P_e/P_a = 1.69$.

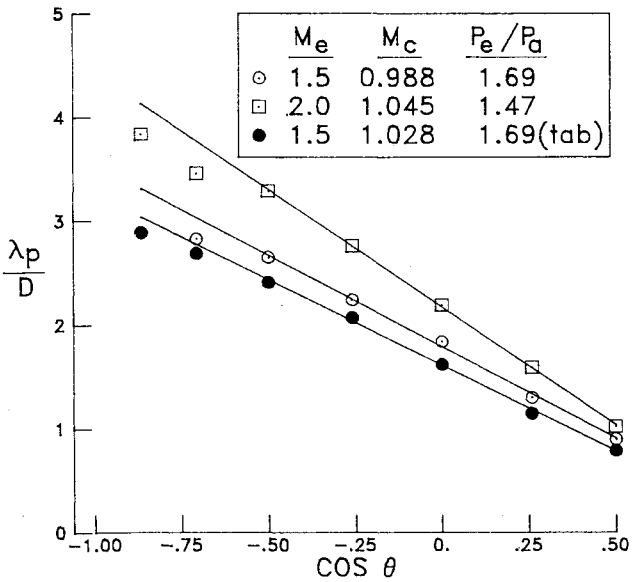

Fig. 8 Variation of peak broadband far-field shock noise frequency with angle-to-jet axis.

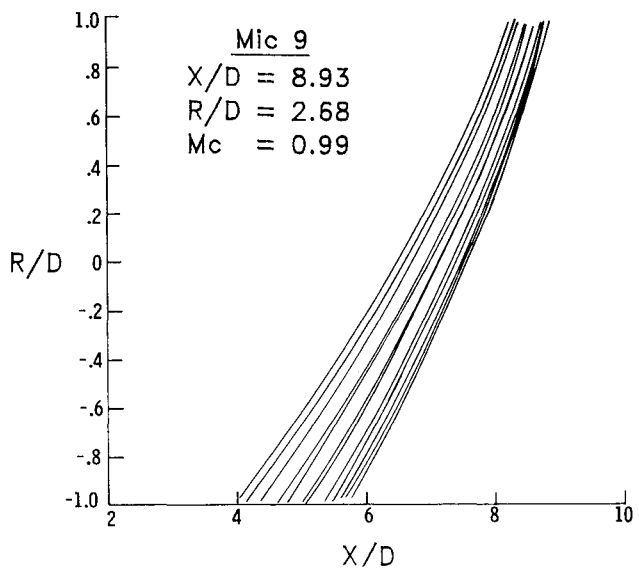

Fig. 9 Optimized time delay curves for fifth shock using $M_c = 0.99$.

factor as $f_p = f_n/(1 - M_c\cos\theta)$. On this basis, then, the convection Mach number can be estimated as

$$M_c = -\frac{\mathrm{d}(\lambda p/D)/\mathrm{d}(\cos\theta)}{\lambda_n/D} \tag{11}$$

where λ_p is the peak acoustic wavelength and D the nozzle diameter. The data of Fig. 8 show how the peak broadband shock noise frequency varies as a function of directional angle for several cases of interest. For the Mach 1.45 nozzle at $P_e/P_a = 1.69$, the far-field acoustic data without screech suppression produce an estimate for the convection Mach number equal to 0.988 with a corresponding convection velocity $U_c = 0.7U_j$. This is a fairly representative convection velocity based on the inflow space-time correlation measurements by Harper-Bourne and Fisher.[4] The Mach 1.99 data show a slightly lower convection velocity relative to the fully expanded jet velocity. From the data of Fig. 8, it is equal to $0.66U_j$.

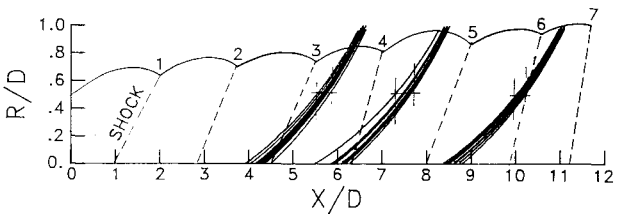

Fig. 10 Optimized time delay curves for several shocks using $M_c = 1.1$.

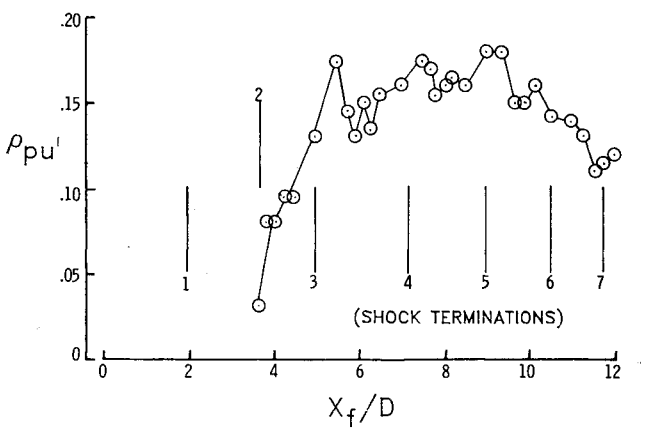

Fig. 11 Pressure-velocity normalized correlation amplitude between hot-film probe and near-field microphone at fourth shock termination.

Figure 9 shows the result of using a convection Mach number of 0.99 in Eq. (10). These data are relevant to measured optimal time delays measured by correlating the hot-film probe with the near-field microphone that has a normal orientation to the fifth shock termination. In this case the number of curves forming possible solutions corresponds to the 13 film probe positions that lie downstream of the microphone's axial location (i.e., $8.2 \le x/D \le 12$). Several other trial convection Mach numbers of 0.9-1.15 were used in an attempt to determine whether a closer grouping of the optimized time delay curves could be obtained. The best grouping of these data occurs with a convection Mach number of 1.1, which is slightly larger than the far-field acoustic estimate of $M_c = 1.03$ for the tabbed related data of Fig. 8. Figure 10 demonstrates the result of using a convection Mach number of 1.1 for three different near-field microphones located at normal observation angles to the fourth, fifth, and seventh shock terminations. For all three of these cases, the optimal time delay curves focus in the vicinity but ahead of the relevant oblique shock nearest the specific near-field microphone. This is generally consistent with those theoretical models that treat the mechanism of broadband shock noise as an interaction between a random vortical flow disturbance and a shock. In Fig. 10, the shock wave pattern for this specific case is denoted by straight lines to assist in interpreting the focused data. As is evident, the data for shock 7 are inconsistent with the other data in that the curves focus much closer to oblique shock 6.

The results of these shock source location measurements are consistent with those observed in Ref. 1 for the Mach 1.99 nozzle with an underexpanded flow at $P_e/P_a = 1.47$. Although no subsonic mixing layer correlations were analyzed in this study, the previous study indicated that good correlation could be obtained only in the supersonic portion of the mixing layer. The subsonic results produced only a small measurable correlation when the data were filtered in the jet noise band.

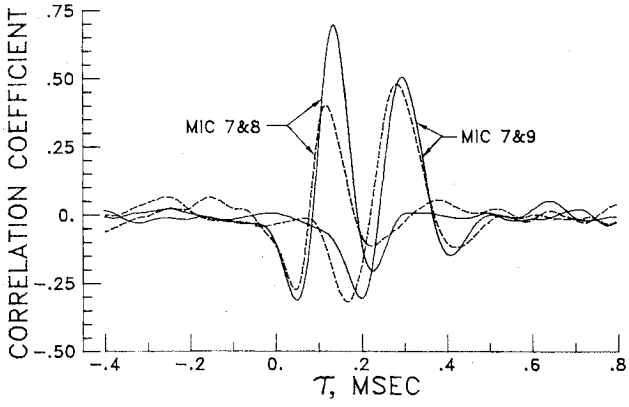

Fig. 12 Comparison between near-field microphone correlations for $M_e = 1.99$ flow (— fully expanded, – – – underexpanded, $P_e/P_a = 1.47$).

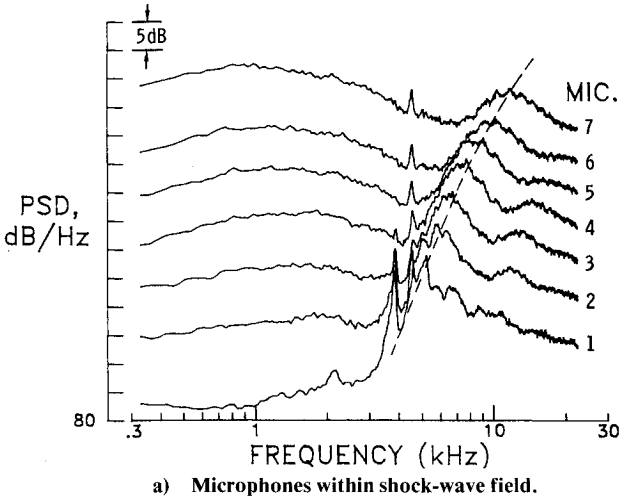

a) Microphones within shock-wave field.

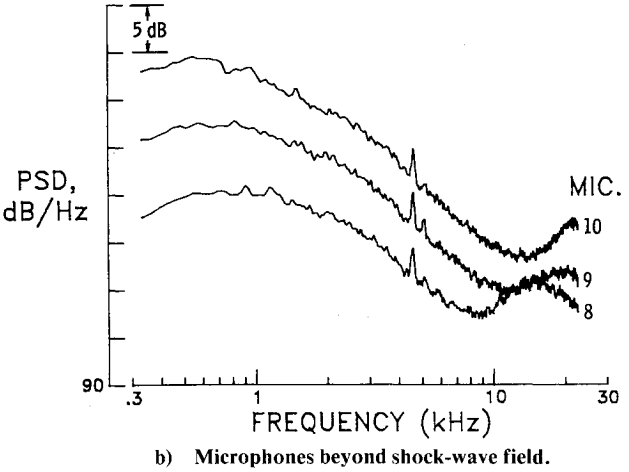

b) Microphones beyond shock-wave field.

Fig. 13 Near-field spectra for $M_e = 1.45$ jet at $P_e/P_a = 0.79$.

The previous study also observed that shock noise generation maintained a good coherence over a large axial extent of the flow. In the present study with the Mach 1.45 nozzle, the same feature is obtained. Figure 11 shows the typical trend using correlations obtained with the microphone near the fourth shock. The data are presented in terms of the normalized correlation coefficient and show only a slow decay in amplitude as the film probe is withdrawn from the vicinity of the fourth shock. The observed decay begins when the film probe is located upstream of the third shock and downstream of the fifth or sixth shock.

The data in Fig. 11 are typical of the measurements from other downstream near-field microphones, which suggests that some large motion exists to collectively interact and phase the action of the downstream shocks. This behavior, if it is present, cannot be observed with the early shock cells, since poor correlations are obtained with them. Thus, while the shock noise is most probably associated with disturbances interacting with an oblique compression shock, the large-scale coherent wave model of Ref. 6 may have an important bearing on details of the overall radiated acoustic shock noise field.

Near-Field Shock Noise Behavior

During the course of this investigation, an interesting feature concerning near-field acoustic behavior was observed for the shock-containing flows. This feature was found to be related to the Doppler factor associated with shock noise that is clearly evident with far-field acoustic behavior such as that of Fig. 8.

The model of Harper-Bourne and Fisher[4] is equivalent to a line array of variable strength monopole sources whose phase is dependent upon the source spacing (shock cell length) and disturbance convection velocity. With such a model, the peak amplitude direction occurs at the Mach angle and is independent of source frequency. Since jet noise dominates radiation to this angle, experimental confirmation is limited. On the basis of this model, the directivity for any given source frequency around the peak angle depends on the individual source amplitudes and the ratio of the acoustic wavelength to the overall dimensions of the phased array. Thus, with the phased linear array model, constructive and destructive acoustic interference effects will produce a dominant group of source frequencies for a particular angle of orientation to the array. In the far field, an observer sees the total integrated effect of the array, since he observes all sources at a similar angle. The far-field observer can therefore detect a Doppler factor with an angle that is solely a function of the phase between sources. In the near field of the sources, typically within one acoustic wavelength of a source, by virtue of his proximity an observer integrates much less of the total phased array properties and has a wide angle of view to the individual sources. On this basis, one would not expect to see the characteristic features of the far-field broadband shock noise spectra or a strong Doppler effect.

On the basis of the above discussion, we were rather surprised to observe near-field spectra with shock noise features of the far-field spectra and an indication of a Doppler factor. In this section we will present these features based on spectra and correlations between near-field microphones. The correlations along with near-field spectra were obtained for both over- and underexpanded cases without the film probe in the flow.

As a starting point in examining the influence of the Doppler factor in the near field, consider the case of the Mach 1.99 nozzle operating at its fully expanded condition. In this case, the entire acoustic field is dominated by jet noise radiation. As indicated by the near-field overall sound pressure level contour plots of Ref. 14, the major direction for this radiation is near $\theta = 30$ deg and appears to originate from a region 8-12 diam downstream of the nozzle exit. Near-field microphone correlations (see Table 1 for the array positions) with microphones beyond $x/D = 4$ indicate that radiation is in the downstream direction, whereas correlation with microphones upstream of this point indicates radiation in the upstream direction. As pointed out in Ref. 1, jet plumes that contain weak shocks do not alter the expected far-field acoustic amplitude and spectral shape for jet noise at its peak radiation angle. Figure 12 shows sample near-field correlations between downstream near-field microphones for the fully expanded case (solid curves) and an underexpanded case containing weak shocks at $P_e/P_a = 1.47$ (dashed curves). These microphones lie within the region of the peak jet noise

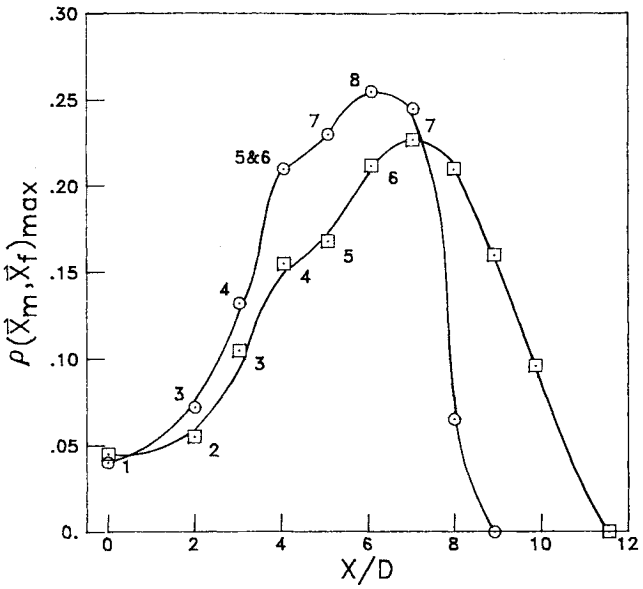

Fig. 14 Major region for broadband shock noise emission for $M_e = 1.45$ flow (○ $P_e/P_a = 0.79$, □ $P_e/P_a = 0.90$; number beside points represent shock termination number).

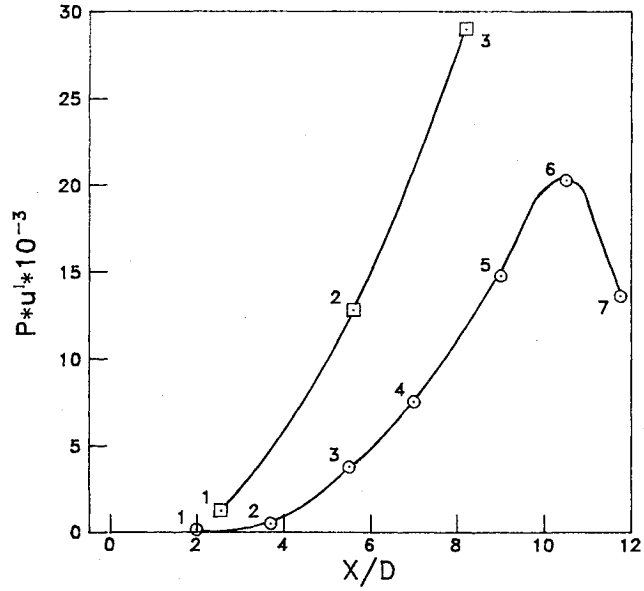

Fig. 15 Major region for broadband shock noise emission from flow-acoustic correlations (○ $M_e = 1.45$, $P_e/P_a = 1.69$; □ $M_e = 1.99$, $P_e/P_a = 1.47$).

radiation, but have also been positioned near the shock terminations. Microphones 7 and 9 are positioned at 90 deg to shock terminations 3 and 4, respectively, while microphone 8 lies midspan between the two and consequently has a different viewing angle than the other microphones to either shock. When the shock-free and shock-containing correlation results are compared, it is evident that the non-normal viewing microphone 8 diminishes the normalized correlation coefficient obtained when no shocks are present in the flow. On the other hand, little deterioration occurs with the normal viewing microphones. Since the jet noise dominates the amplitude and spectra of both the shock-free and shock-containing cases, evidently microphone 8 picks up some additional noise that is uncorrelated with the processes at shock positions 3 and 4. This would be expected if the additional noise source, in this case broadband shock noise, produced radiation with a Doppler factor. In this way correlations between the microphones with varying observation angles to the shocks would diminish the measured correlation due to a shift of frequency with the observation angle. Similar observations can also be made between the correlations of the downstream microphones for the Mach 1.45 jet operating underexpanded at $P_e/P_a = 1.69$.

While the data for these two nozzle cases are limited, the results do suggest that a Doppler effect may be operational in the near field of the shock noise sources. This would occur if these sources were emitting sound while being convected by the mean flow. In the overexpanded cases investigated with the Mach 1.45 jet, near-field spectra show clearly characteristic broadband shock noise peaks. Figure 13 shows these near-field spectra for the overexpanded condition of $P_e/P_a = 0.79$. Here we see that for microphones 1-6, which lie within the axial extent of the shock-wave field, the peak broadband shock noise frequency shifts with location relative to the shock-wave field. For microphones 7-11, which are located beyond the shock-wave field, one can observe that this trend continues, but it could be predicted by a phased array model since these microphones begin to view all the shocks at similar angles. However, these downstream microphones reveal that significant broadband shock noise energy is propagating in the jet arc, since they are all located beyond the shock-wave field.

Dominant Region for Shock Noise

In both Refs. 1 and 12 it was shown that the downstream shocks play a fundamental role in broadband shock noise emission. The overexpanded cases of $P_e/P_a = 0.79$ and 0.90 for the Mach 1.45 nozzle provide a convenient means for estimating the region for dominant shock noise emission. This can be achieved through correlation of the near-field microphones with a set of far-field microphones in and around the peak broadband shock noise frequency of the far-field microphone. In this investigation this was performed using only a far-field microphone at 90 deg to the jet axis, but in general, the correlation should be applied with microphones at varying angles. Figure 4 shows the typical far-field spectra for the $P_e/P_a = 0.79$ condition around which filtered correlations were obtained using the screech suppression method described previously. A similar filtered band was used at the $\beta = 0.94$ condition. Figure 14 shows the variation of the normalized correlation coefficient as a function of the microphone's axial location for these two overexpanded conditions. The numbers beside the symbols refer to those shocks where the respective microphone has a 90-deg orientation to a shock termination like that of the far-field microphone. It is evident from these data that several shock interactions are of importance, all of which occur with the last several shocks in the shock-wave field.

In the underexpanded cases, the jet noise component severly interfers with the coherence levels obtained by a near/far-field correlation, even though the far-field microphone exhibits a strong shock noise peak frequency. The inflow correlations with near-field microphones do provide a means for estimating the regions for maximum contribution to shock noise. The data of Fig. 15 show this in terms of the correlation function in physical units between the hot-film probe and the near-field microphone near each shock termination. It can be observed for the Mach 1.45 nozzle's results that the maximum contribution to the shock noise occurs from these downstream shocks. The trend is similar for the Mach 1.99 nozzle, although the data range is too limited to be conclusive.

Comparison of the overexpanded and underexpanded results of Figs. 14 and 15 indicate that the maximum production of broadband shock noise occurs at different locations in their respective shock-wave field. Common to both conditions and nozzles, however, is that this region for maximum shock noise production occurs in the vicinity of each flow's end of the initial mixing layer. This is the region

where large-scale instabilities have reached their maximum growth before decay[6,14] and possibly influence the shock noise production mechanism.

Conclusions

The principle findings of the experimental study are as follows:

1) The major region for broadband shock noise production occurs in the vicinity of the end of the jet plume's initial mixing region for both under- and overexpanded supersonic jets.

2) Flow and near-field acoustic correlations indicate a spatial coherence of at least several shock wavelengths.

3) Near-field spectra exhibit a Doppler effect within an acoustic wavelength of the source or source array dimension.

4) Broadband shock noise is radiated at small angles to the jet axis.

5) Shock noise appears to originate from the vicinity of each oblique shock in the jet plume's shock-wave field.

6) Longitudinal turbulent velocity fluctuations dominate temperature fluctuations in a shock-containing unheated supersonic jet.

These results at least indicate that broadband shock noise is produced by the discrete interaction of flow disturbances and a shock, but that the large-scale flow disturbances provide a certain degree of phasing for the sound emitted from each individual shock interaction. The large-scale coherent-like structures,[6] with a scale near the downstream shock wavelength, achieve their maximum growth in the vicinity where peak broadband shock noise appears to be emitted.

The apparent Doppler effect in the near field suggests that the observed Doppler shift in acoustic far-field data may originate from source convection effects rather than from the effect of a phased array. In a supersonic flow, shock positions cannot be considered stationary when propagating into a region with time-dependent disturbances.

Wedge hot-film aerodynamic measurements have shown that the growth of the turbulent mixing layer is strongly modulated by a shock-wave field. This modulation appears to be governed by variations to the mean flow produced by the shocks. Maximum turbulence intensity levels for the longitudinal component occur near the end of the compression zones and minimum levels near the end of expansion zones. The present results show no indication to a modification of the turbulence structure immediately downstream of a weak shock.

References

[1] Seiner, J. M. and Norum, T. D., "Aerodynamic Aspects of Shock Containing Jet Plumes," AIAA Paper 80-0965, 1980.

[2] Lighthill, M. J., "On Energy Scattered from the Interaction of Turbulence with Sound or Shock Waves," *Proceedings of the Cambridge Philosophical Society*, Vol. 49, 1953, pp. 531-551.

[3] Ribner, H. S., "Acoustic Energy Flux From Shock-Turbulence Interaction," *Journal of Fluid Mechanics*, Vol. 25, Pt. 2, 1969, pp. 299-310.

[4] Harper-Bourne, M. and Fisher, M. J., "The Noise from Shock Waves in Supersonic Jets," AGARD CP 131, 1973, pp. 1-13.

[5] Howe, M. S. and Ffowcs Williams, J. E., "On the Noise Generated by an Imperfectly Expanded Supersonic Jet," *Philosophical Transactions of the Royal Society of London*, Vol. 289, No. 1358, 1978, pp. 271-314.

[6] Tam, C. K. W. and Tanna, H. K., "Shock Associated Noise of Supersonic Jets from Convergent-Divergent Nozzles," *Journal of Sound and Vibration*, Vol. 83, 1981, pp. 337-358.

[7] Pao, S. P. and Seiner, J. M., "Shock Associated Noise in Supersonic Jets," *AIAA Journal*, Vol. 21, May 1983, pp. 687-693.

[8] Seiner, J. M., "The Wedge Hot-Film Anemometer in Supersonic Flow," NASA TP 2134, May 1983.

[9] Morkovin, M. V., "Fluctuations and Hot-Wire Anemometry in Compressible Flows," AGARD No. 24, 1956.

[10] Rose, W. C., "The Behavior of a Compressible Turbulent Boundary Layer in a Shock-Wave Induced Adverse Pressure Gradient," NASA-TN-D-7092, 1973.

[11] Stone, J. R., "Interim Prediction Method for Jet Noise," NASA TMX-71618, 1974.

[12] Norum, T. D. and Seiner, J. M., "Broadband Shock Noise from Supersonic Jets," *AIAA Journal*, Vol. 20, Jan. 1982, pp. 68-73.

[13] Pao, S. P. and Salas, M. D., "A Numerical Study of Two-Dimensional Shock Vortex Interactions," AIAA Paper 81-1205, 1981.

[14] Seiner, J. M., McLaughlin, D., and Liu, C. H., "On the Noise Generated by Large Scale Instabilities in Supersonic Jets," NASA TP 2072, 1982.